Stellar neutron capture on $^{180}Ta^m$. I. Cross section measurement between 10 keV and 100 keV

K. Wisshak,* F. Voss, C. Arlandini, F. Käppeler, and M. Heil
Forschungszentrum Karlsruhe, Institut für Kernphysik, Postfach 3640, D-76021 Karlsuhe, Germany

R. Reifarth
Los Alamos National Laboratory, Los Alamos, New Mexico 87545, USA

M. Krtička and F. Bečvář
Faculty of Mathematics and Physics, Charles University, CZ-180 00 Prague, Czech Republic
(Received 17 February 2003; revised manuscript received 9 December 2003; published 11 May 2004)

The neutron capture cross section of $^{180}Ta^m$ has been measured at energies between 10 keV and 100 keV in a time-of-flight experiment at the Karlsruhe 3.7 MV Van de Graaff accelerator. Neutrons were produced via the $^7Li(p,n)^7Be$ reaction by bombarding metallic Li targets with a pulsed proton beam, and gold was used as a cross section standard. Though the world supply of enriched $^{180}Ta^m$ was available for this experiment, the sample consisted of only 150 mg Ta_2O_5 with a $^{180}Ta^m$ content of only 5.5%. The difficult separation of the comparably few capture events in $^{180}Ta^m$ from the much larger background due to captures in ^{181}Ta could be achieved by means of the Karlsruhe 4π barium fluoride detector, taking advantage of its combination of high efficiency, good energy resolution, and high granularity. The cross section was determined with an overall uncertainty of better than 10% in the energy range from 30 keV to 100 keV and could be used for renormalizing statistical model calculations in the entire energy range of astrophysical interest, which had predicted about two times larger values. Based on these first experimental data, Maxwellian averaged neutron capture cross sections were calculated for thermal energies between $kT=8$ keV and 100 keV.

DOI: 10.1103/PhysRevC.69.055801 PACS number(s): 25.40.Lw, 26.20.+f, 27.70.+q, 97.10.Cv

I. INTRODUCTION

Over the past 25 years $^{180}Ta^m$ has attracted great interest for reasons related to nuclear and astrophysical aspects: It is the rarest stable isotope found in the solar system, representing only 0.012% of natural tantalum (which in turn is the rarest chemical element in nature [1]), and it is the only isotope that is stable in the isomeric state. Though its complicated origin and its peculiar nuclear structure triggered numerous investigations, the related quests turned out to be rather difficult to answer, making this subject, indeed, a tantalizing field of research.

The rarity of $^{180}Ta^m$ reflects the difficulty of its production. At first, the common processes for synthesizing the heavy elements, including the *s*, *r*, and *p* processes, even seemed to fail in this case. Apart from the difficulty in producing it, $^{180}Ta^m$ may be even easily destroyed in the hot stellar interior by thermally induced depopulation to the short-lived ground state. Obviously, $^{180}Ta^m$ owes its existence to a fine balance of nuclear and stellar parameters. Therefore it is long recognized to represent an important test for nucleosynthesis models of the heavy elements and attracted continuous efforts in experimental nuclear physics as well as in theoretical astrophysics. For the crucial nuclear part experiments were severely hampered by the lack of enriched samples and/or sufficiently sensitive techniques, often allowing only qualitative statements to be made. This challenge motivated a whole series of recent approaches aiming at more quantitative solutions. Among the various nucleosynthesis mechanisms, the *s* process is certainly most suited for a quantitative description of the corresponding $^{180}Ta^m$ yield, since the reaction path follows the valley of β stability and is, therefore, directly accessible to laboratory studies. Also from the astrophysical side the associated He burning scenarios are comparably stable and easier to model than the explosive scenarios responsible for the *r* and *p* processes.

The (n,γ) measurements required for defining the *s*-process contribution to $^{180}Ta^m$ are described in Sec. II, followed by the data analysis procedures (Sec. III) and a discussion of the results and uncertainties (Secs. IV and V). The astrophysical aspect is introduced in Sec. VI, where the stellar cross sections are determined. A detailed description of the technical part, including the data obtained in individual runs and with different evaluation methods, as well as the calculation of correction factors and a more detailed description of the computer simulations can be found in Ref. [2]. The main experimental results and a brief discussion of the astrophysical interpretation have been published already in Ref. [3].

II. EXPERIMENT

The neutron capture cross section of $^{180}Ta^m$ was measured in the energy range from 10 keV to 100 keV using gold as a standard. Since the experimental method has been published in detail [4–7], only a general description is given here, complemented with the specific features of the present measurement.

*Corresponding author. Email: klaus.wisshak@ik.fzk.de

TABLE I. Sample characteristics.

Sample	Diameter (mm)	Thickness (mm)	Thickness (10^{-3}at/b)[c]	Weight[a] (g)	Container[b] (g)	Neutron binding energy (MeV)
Empty						
^{197}Au	11.5	0.125	0.7427	0.2523	1.8343	6.513
^{180}Ta^m	11.5	0.7	0.3939	0.1501[d]	1.8708	7.538
^{181}Ta	11.5	0.7	0.3933	0.1499	1.7680	6.063
Dummy					1.8702	

[a]For tantalum samples: weight of Ta_2O_5.
[b]Graphite container, diameter 22 mm, thickness 3 mm.
[c]For tantalum samples: sum of both Ta isotopes.
[d]Isotopic composition: ^{180}Ta^m 5.47±0.05%, ^{181}Ta 94.53±0.05%.

Neutrons were produced via the ^{7}Li$(p,n)^7$Be reaction by bombarding metallic Li targets with the pulsed proton beam of the Karlsruhe 3.7 MV Van de Graaff accelerator. The neutron energy was determined by time of flight (TOF), the samples being located at a flight path of 79 cm. The relevant parameters of the accelerator were a pulse width of <1 ns, a repetition rate of 250 kHz, and a typical average beam current of 1.8 μA. The measurement was carried out in two runs with the proton energy adjusted 20 keV and 30 keV above the threshold of the ^{7}Li$(p,n)^7$Be reaction at 1.881 MeV, resulting in continuous neutron spectra in the energy range from 10 keV to 80 keV and 5 keV to 100 keV, respectively. The neutron beam was collimated to a diameter of 15 mm at the sample position.

Capture events were registered with the Karlsruhe 4π BaF_2 detector via the prompt capture γ rays. This detector consists of 29 hexagonal and 12 pentagonal crystals forming a spherical shell of BaF_2 with 10 cm inner radius and 15 cm thickness. It is characterized by a resolution in γ ray energy of 7% at 2.5 MeV, a time resolution of 500 ps, and a peak efficiency of 90% at 1 MeV. The 1.7 MeV γ ray threshold used in the sum-energy spectrum corresponds to an efficiency for capture events of more than 95%. (For a comprehensive description of this detector see Ref. [6].) In both experimental runs the conventional data acquisition technique was used with the detector operated as a calorimeter.

The present experiment was carried out with the same ^{180}Ta^m sample that had been previously used in the photoactivation experiment [8,9]. Though it represented the world supply of isotopically enriched Ta_2O_5, it consisted of only 150 mg with a ^{180}Ta^m content of 5.5%. This total amount of 6.7 mg ^{180}Ta^m was significantly less than the 500 mg typically used in this type of cross section measurements. The sample of 11.5 mm diameter and 0.7 mm thickness was encapsulated in a flat graphite container. Identical containers were also used for a set of additional samples mounted on a sample ladder. This set included a gold disk for determining the neutron flux, 150 mg natural tantalum oxyde for obtaining the isotopic correction, as well as an empty container for simulating the background due to scattered neutrons and for measuring the background related to the container itself. Furthermore, an empty position on the sample ladder allowed us to determine the sample-independent background. The relevant data characterizing these samples are compiled in Table I.

Because of the enormous value of the enriched material, the container was designed for the safe handling of the sample during the related photoactivation study and could not be optimized for the present experiment. Accordingly, there were 100 times more carbon than tantalum atoms in the neutron beam. If the ^{180}Ta^m content is taken into account, this means that 6000 neutrons were scattered by the graphite container per capture event in ^{180}Ta^m. The corresponding background due to captures of scattered neutrons in the BaF_2 crystals could be sufficiently reduced by the unique combination of high efficiency, good energy resolution, and TOF discrimination provided by the present setup. In view of this difficulty, the run with 100 keV maximum neutron energy was complemented by a run with a maximum energy of 80 keV, resulting in a reduced integral neutron flux. Since this change left the flux around 30 keV unaltered, the signal-to-background ratio in the important energy range from 20 keV to 50 keV could be significantly improved.

The samples were put cyclically into the measuring position by a computer controlled sample changer. The measuring time per sample of typically 10 min was defined by a beam current integrator. Long-term variations of the neutron yield were compensated by averaging over 400–600 cycles per run. Sum energy, TOF information, and identity of the responding detector modules were recorded for each event. In the following, the multiplicity m denotes the number of detector modules responding per event. Because of cross talk between modules, the instrumental γ multiplicity m is slightly larger than the true cascade multiplicity m'.

The experiment was restricted to the so-called calorimeter mode, because the small sample mass did not allow us to achieve the counting statistics required for the analog-to-digital-convertor (ADC) mode where the signals of all detector modules are recorded individually.

The total measuring time was 17.3 and 27.2 days beam on target for the runs with a maximum neutron energy of 100 keV and 80 keV, respectively. The average beam current was between 1.6 and 2.0 μA [2].

III. DATA ANALYSIS

The analysis of measured data and the determination of the neutron capture cross section has been described in detail in previous publications [4,5,7]. Therefore, the following dis-

cussion will focus on the particular situation of the present measurement.

A. Simulations

In order to provide a physically sound basis for the quantitative analysis of the multiparametric data on γ-cascades measured with the Karlsruhe 4π BaF_2 detector, we elaborated two dedicated codes, CASINO [10] for simulating the γ cascade following keV-neutron capture in the region of unresolved resonances, and a GEANT-based code [11] for imitation of the response of the detector modules to these γ cascades. Both codes were used in our analysis of the data from the $^{180}Ta^m$ sample.

The CASINO code is an implementation of the DICEBOX algorithm for artificially generating capture cascades consisting of γ rays and conversion electrons from the decay of a fixed highly excited nuclear level with known spin and parity. This algorithm is based on the main postulates of the extreme statistical model of the nucleus and on the paradigm of the photon strength functions. As it mimics the Markovian character of cascade emission, it allows one to keep the uncertainties associated with Porter-Thomas fluctuations of partial radiation and reduced neutron widths under control [12].

The CASINO code takes the energy spectrum of the incident neutron beam as well as the distribution of the energy- and spin-dependent strengths of participating *s*- and *p*-wave neutron resonances into account. The input information for CASINO is represented by (i) the neutron strength functions for *s*- and *p*-wave neutrons, (ii) the parameters of the photon strength functions and of the level density, and (iii) the accessible data on decay properties of low-lying levels of the product nucleus. In each run, CASINO yields typically 200 000 cascades, each being characterized by a set of conversion-electron and γ-ray energies.

The GEANT-based code [11] reproduces all relevant interactions of the emitted radiation with the scintillators and the passive material of the whole 4π BaF_2 detector. The fate of each γ ray is traced in detail from its origin up to its complete absorption or escape from the system, respectively. The geometry of the Karlsruhe 4π BaF_2 array is carefully modeled, describing the shape of the 41 crystals and of all structural details. The efficiency for γ rays from the sample in the center of the detector is calculated including the corrections for γ ray self-absorption, and the energy resolution corresponds to experimentally measured data recorded with an ADC system. Furthermore, the experimental threshold of 50 keV per module was properly considered.

In this way, the response of the 4π BaF_2 array to the cascades produced by the CASINO code could be studied in detail, thus providing a complete simulation of the experiment. In particular, it was possible to obtain sum-energy spectra for various instrumental γ multiplicities *m*. These observables could in turn be confronted with the corresponding experimental data or used for their analysis.

B. Background subtraction

All recorded events were sorted into two-dimensional spectra containing 128 sum energy versus 2048 TOF channels according to various event multiplicities (evaluation 1). In evaluation 2, this procedure was repeated by rejecting events where only neighboring detector modules contributed to the sum-energy signal. With this option, background from the natural radioactivity of the BaF_2 crystals and from scattered neutrons has been reduced. The corresponding loss of true events has been corrected as described in Ref. [13]. The uncertainty of this correction is small and is included in the systematic uncertainty of the correction F_1.

The resulting spectra were normalized to equal neutron flux using the count rate of a ^6Li glass monitor close to the neutron target. In all runs and for all samples the respective normalization factors differed by less than 0.5% from unity.

It turned out that the γ cascades from neutron capture on $^{180}Ta^m$ exhibit an average instrumental multiplicity $\langle m \rangle = 6.2$, by far the largest value ever measured with the Karlsruhe 4π BaF_2 detector. Since spin and parity of $^{180}Ta^m$ are 9^-, the values of J^π for the dominating *s*- and *p*-wave neutron capturing levels of the system $^{180}Ta^m + n$ are $15/2^+$, $17/2^\pm$, $19/2^\pm$, and $21/2^+$. On the other hand, spin and parity of the ^{181}Ta ground state are $7/2^+$. Having in mind that *E*1 and *M*1 transitions strongly prevail in neutron-induced γ production, emission of cascades with true multiplicities $m' < 4$ are significantly suppressed. Indeed, the multiplicity of the shortest cascade, formed exclusively by *E*1 and/or *M*1 transitions, is $m' = 4$. This accounts for the large value of the instrumental multiplicity.

This feature allowed us to evaluate the $^{180}Ta^m$ cross section using only events with multiplicities $m \geqslant 5$, which are much less affected by background contributions than events with lower multiplicities. In this way we could compensate to some extent the rather poor signal-to-background ratio due to the small sample and the dominant parasitic capture on ^{181}Ta. The missing fraction of low multiplicity events was determined by means of the computer simulation described below.

Capture events from the dominant ^{181}Ta impurity could be additionally discriminated because of the smaller *Q* value of 6.1 MeV, resulting in a sum-energy peak well below that of $^{180}Ta^m$ at 7.6 MeV.

In the next step of data analysis, sample-independent background contributions were removed by subtracting the spectrum measured with the empty position in the sample ladder. A remaining constant background was determined at very long flight times where no time-correlated events are expected. This minor component is due to small differences in the overall background, which result from the different scattering effects of the samples used.

At this point, the resulting spectra contain only events correlated with the sample. The following correction for isotopic impurities (see Ref. [4] for details) was performed by subtracting the spectrum of the natural tantalum sample after normalization to equal number of atoms. This step accounted also for most of the background from scattered neutrons, which is dominated by the graphite can. Figure 1 shows the projection of the $^{180}Ta^m$ spectrum for neutron energies between 40 keV and 75 keV (vertical lines in Fig. 2) onto the sum-energy axis before and after subtraction of the background from isotopic impurities. The uncorrected spectrum (top) is clearly dominated by background peaks from neutron

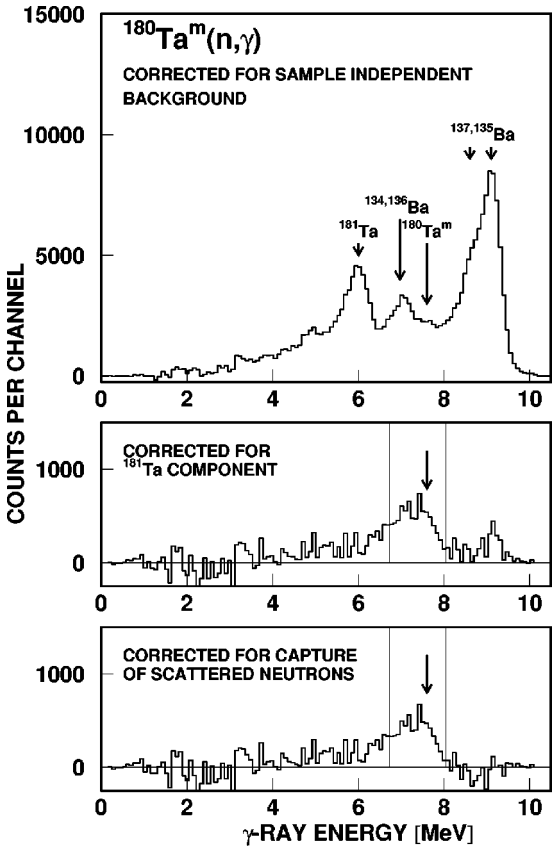

FIG. 1. Sum-energy spectra of the $^{180}Ta^{m}$ sample before and after the subtraction of the background components due to capture events in the ^{181}Ta impurity and due to capture of scattered neutrons (data from run II only). The energy range between 6.8 MeV and 8 MeV that was used to determine the cross section as a function of neutron energy is indicated by vertical lines. The spectra were obtained by integration over the neutron energy range from 40 to 75 keV as indicated in Fig. 2. All spectra refer to multiplicity >4.

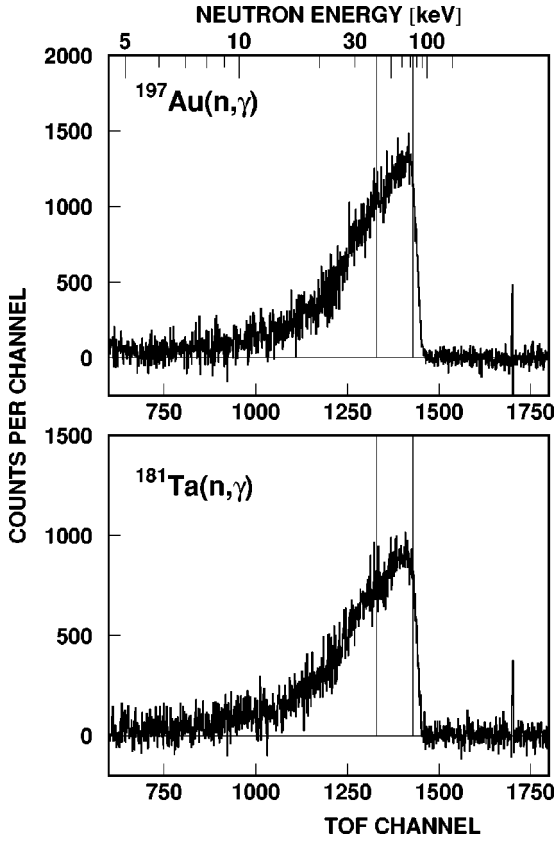

FIG. 2. The background-corrected TOF spectra of the ^{197}Au and ^{181}Ta samples from run II with 80 keV maximum neutron energy used for determination of the cross section as a function of neutron energy. The regions for absolute normalization of the cross section and for the projections shown in Figs. 1, 4, and 5 are indicated by vertical lines.

captures on the abundant ^{181}Ta impurity and from captures of scattered neutrons on the odd and even barium isotopes of the scintillator. The small peak due to capture on $^{180}Ta^{m}$ becomes evident in the corrected spectrum in the middle part of Fig. 1.

The occurrence of converted transitions was recently found responsible for the broadening of the sum-energy peak in the spectrum of the gold standard (see below) [14]. In high Z materials such as gold and tantalum, large cascade multiplicities may imply a certain fraction of soft γ transitions with sizable conversion coefficients. Since the conversion electrons are easily absorbed before reaching the scintillator, their energy is missing in the recorded signals, resulting in a broadening of the sum-energy peak. Note that this effect corresponds to a reduction of the effective cascade energy. Experiments with the 4π BaF_2 detector are not affected by this problem, since the detection efficiency is completely independent of the corresponding minor loss in resolution.

In principle, the population of isomeric levels may also cause some broadening in sum-energy spectra, as shown in case of neutron capture in several ytterbium isotopes [15]. If capture γ-ray cascades populate a level with a half-life longer than the experimental coincidence interval of about 30 ns, the depopulating transitions to the ground state will not contribute to the sum-energy signal. So far, only one level at 482 keV is known in ^{181}Ta with a half-life of 10 ns, too short to cause the observed effect in the case of neutron capture in $^{180}Ta^{m}$.

The energy dependence of the $^{180}Ta^{m}$ cross section is evaluated only from events with sum energies near the full energy peak as indicated in Fig. 1 by vertical lines. This region lying well above the capture events in ^{181}Ta ensures that background due to capture of scattered neutrons is properly corrected by subtraction of the normalized spectrum of the ^{181}Ta sample.

The correction for isotopic impurities accounted also for most of the background due to capture of sample scattered neutrons originating mostly from the comparably massive graphite container. Fortunately, the binding energy of both investigated isotopes is below 8 MeV, thus allowing us to use the strong peak due to capture in the odd barium isotopes between 8 MeV and 10 MeV for normalization. The remaining background from scattering on the $^{180}Ta^{m}$ sample itself required only a small additional correction and is shown in the lower part of Fig. 1. Since this normalization is determined as a function of neutron TOF, the correction for scat-

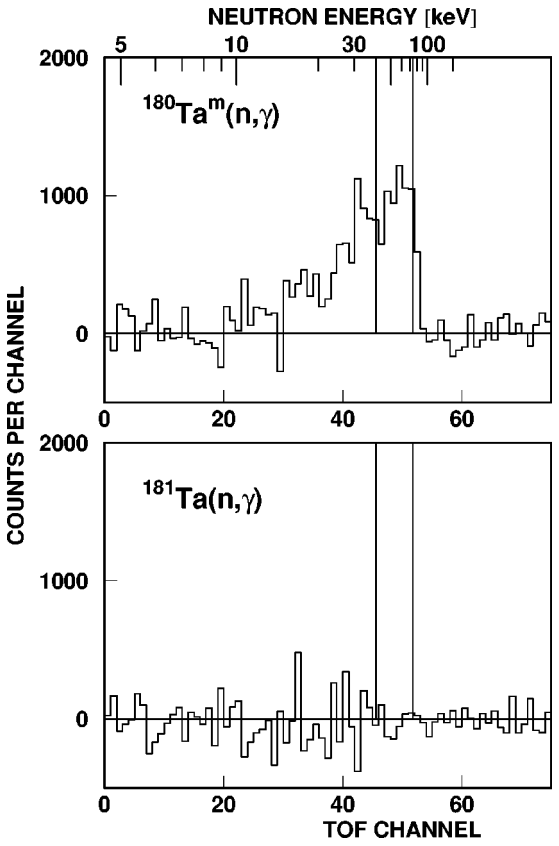

FIG. 3. The background-corrected TOF spectrum of the $^{180}Ta^{m}$ sample from run II with 80 keV maximum neutron energy (top panel). The original bin size was increased by a factor of 16 to better visualize the TOF spectrum of $^{180}Ta^{m}$. The region for absolute normalization of the cross section is indicated by vertical lines. The bottom panel shows the respective TOF spectrum measured with the natural tantalum sample integrated over the same sum-energy range from 6.8 to 8 MeV (see Fig. 1). The absence of any time-correlated events illustrates the efficient background suppression via the sum-energy information.

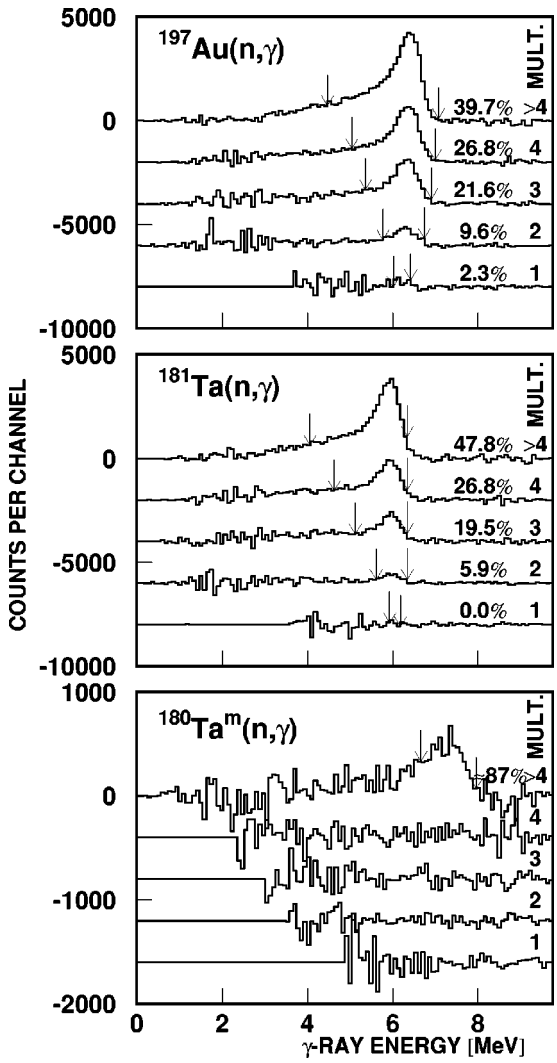

FIG. 4. Sum-energy spectra of all isotopes as a function of multiplicity (data from run II only). For better readability the different spectra are displaced by 2000 and 400 counts per channel, respectively (channels with dominant statistical uncertainties are suppressed). The regions used to determine the cross section shape (see Figs. 2 and 3) are indicated by arrows. For $^{180}Ta^{m}$ only events with multiplicity >4 were used in the evaluation.

tered neutrons is accurately treated in the entire energy range of this experiment. After this last step, the spectra contain only capture events on the investigated isotopes.

The final TOF spectra in Figs. 2 and 3 were used to determine the cross section shape. Since the cross sections of ^{181}Ta and ^{197}Au exhibit to good approximation a $1/v$ dependence, the TOF spectra of both isotopes are practically identical to the previous experiment [7] that was carried out with much larger samples and, consequently, much better statistics. The agreement confirms the reliability of the present data.

The TOF scale of the corresponding spectrum for the $^{180}Ta^{m}$ sample (upper part of Fig. 3) is compressed by a factor 16 in order to reduce statistical fluctuations. In spite of the comparably low number of counts it is evident that the spectrum shape equals that of the other samples. The lower part of Fig. 3 shows the projection for the natural ^{181}Ta sample in the same sum-energy interval from 6.8 MeV to 8 MeV (see Fig. 1). The evident lack of capture events in the resulting spectrum provides an impressive confirmation for the selectivity of the combined TOF and sum-energy information.

C. Detection efficiency for capture events on $^{180}Ta^{m}$

The two-dimensional data were projected onto the sum-energy axis using the TOF region with optimum signal-to-background ratio indicated in Figs. 2 and 3 by vertical lines. The resulting sum-energy spectra are plotted in Fig. 4 for different multiplicities m. The arrows in Fig. 4 indicate the range of sum-energy channels that were integrated to obtain the TOF spectra of Figs. 2 and 3 for determining the cross section shape.

The multiplicity distributions for $^{180}Ta^{m}$ and ^{181}Ta exhibit remarkable differences. Only 40% and 50% of the capture events in the ^{197}Au and ^{181}Ta sample are observed with in-

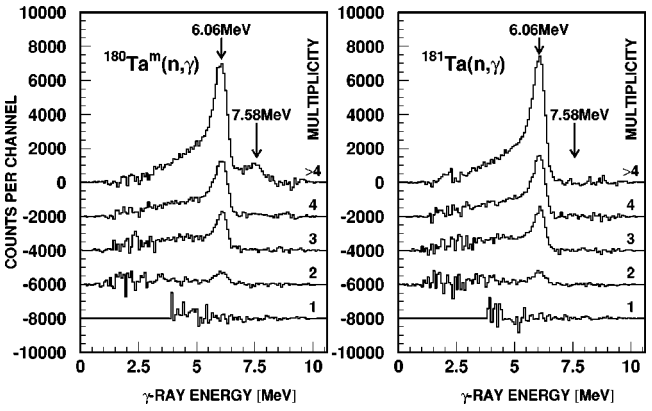

FIG. 5. Sum-energy spectra of both tantalum samples as a function of multiplicity (channels with dominant statistical uncertainties are suppressed). These spectra represent the data of both runs and were obtained without correction for isotopic impurities.

strumental multiplicities $m \geqslant 5$, while the respective fraction is $87 \pm 5\%$ for ^{180}Ta^m. This fraction of ^{180}Ta^m events, which was obtained from the spectra of Fig. 4, could be well reproduced by means of a computer simulation as described below.

The final uncertainty of the measured ^{180}Ta^m cross section is dominated by counting statistics and by the fraction of detected events. The integration of the sum-energy spectrum from the experimental threshold at 1.7 MeV up to 8 MeV (bottom panels of Figs. 1 or 4), which is required for determining the absolute value of the cross section, is affected by large statistical uncertainties due to the backgrounds from the

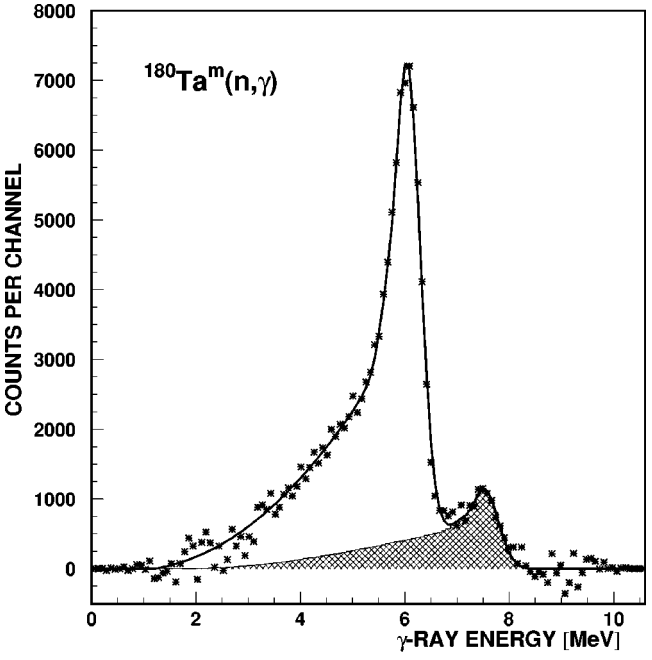

FIG. 6. Sum-energy spectrum of the enriched tantalum sample without correction for isotopic impurities (events with multiplicity $m > 4$ only, see Fig. 5). The experimental data (stars) are fitted by the procedure described in the text (solid line). The separation of capture events on ^{181}Ta and on ^{180}Ta^m is illustrated by the hatched area, which describes the latter component.

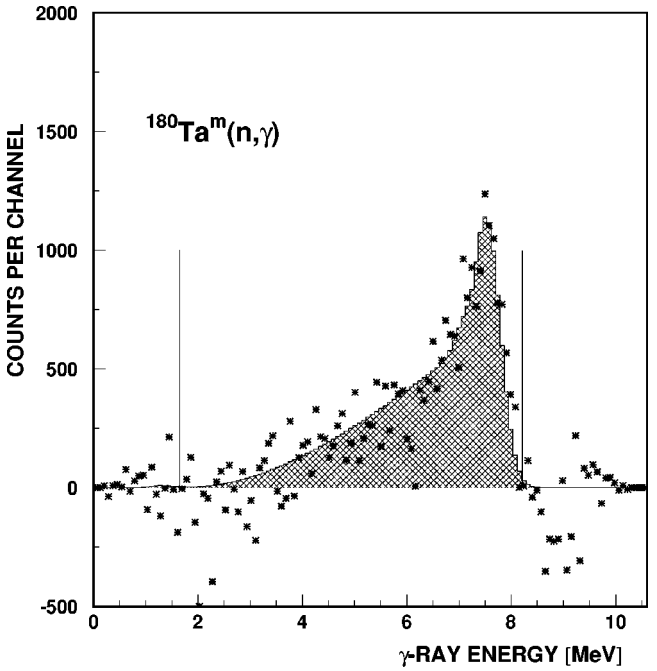

FIG. 7. The sum-energy spectrum of ^{180}Ta^m obtained by subtraction of the ^{181}Ta component (stars). This spectrum is in good agreement with the independent result shown in Fig. 6 (hatched area).

^{181}Ta impurity (mainly at 6–7 MeV) and from natural radioactivities (up to 4 MeV). Since only events with multiplicities $m \geqslant 5$ could be recorded with sufficient signal-to-background ratio (Fig. 4), this fraction had to be determined more reliably.

1. Isotopic separation

The data were reanalyzed without applying the correction for isotopic impurities. The spectra taken with the empty graphite container were normalized via the pronounced Ba peaks (Fig. 1). In this way, the large background due to neutrons scattered by the graphite container was eliminated. The resulting spectra are shown in Fig. 5 for the natural and the enriched tantalum sample.

The ^{180}Ta^m and ^{181}Ta components in the spectrum of the enriched sample were separated by a fitting procedure [15] based on the previously measured sum-energy spectra of about 20 isotopes covering a range of neutron separation energies between 4.78 MeV (^{232}Th) to 8.34 MeV (^{155}Gd). These spectra were fitted by a Gaussian for the full energy peak and a truncated polynomial for the low energy tail. With the systematics of these fit parameters it was found that the intensity ratio of the full energy peak and the low energy tail could be reliably determined from the respective neutron separation energy.

The decomposition of the spectrum taken with the enriched sample (left panel of Fig. 5) was facilitated since the shape of the ^{181}Ta component could be adopted from the spectrum of the natural sample (right panel of Fig. 5). The shape of the ^{180}Ta^m component was determined by means of the parameter systematics. The fit of these two components

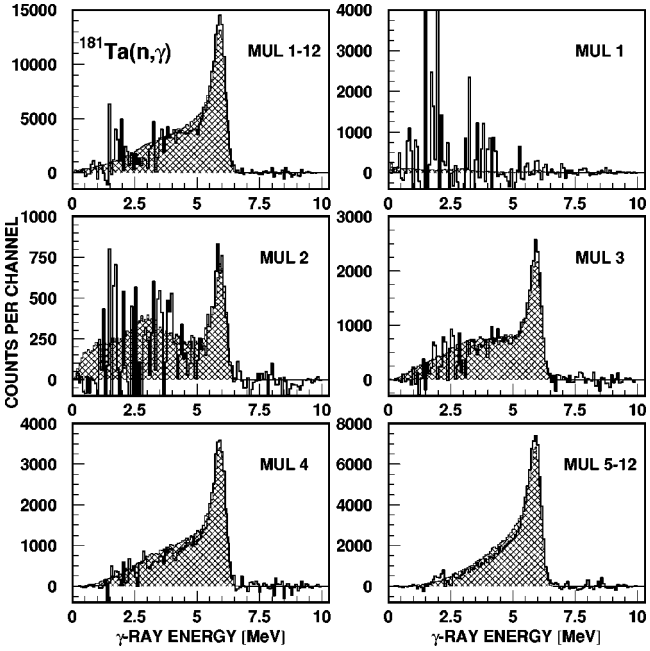

FIG. 8. Comparison of the simulated spectra for multiplicity 1–12 (dashed areas) and the measured spectra of Fig. 5 (histograms) illustrating that both, the spectral shapes and the relative contributions, are well reproduced by the simulation. The only adjustment of the simulation was to match the total spectrum in the upper left corner.

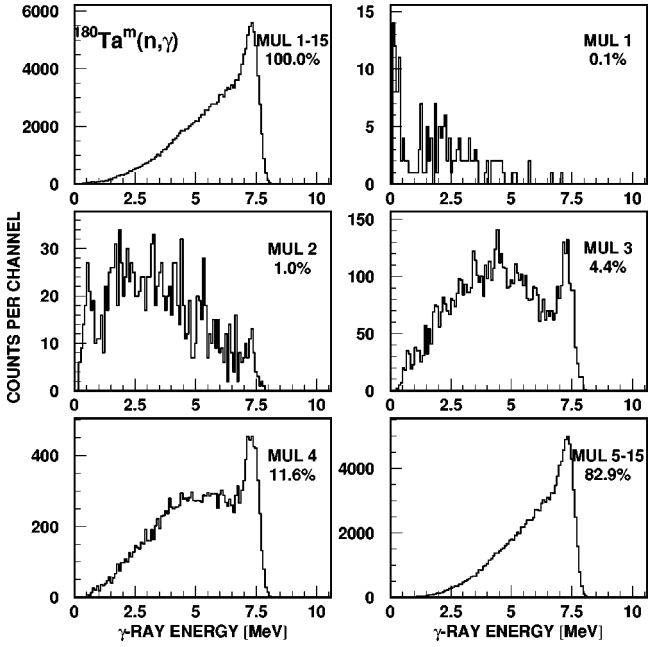

FIG. 9. Simulated sum-energy spectra for neutron capture on $^{180}Ta^{m}$. The 83% contribution of the spectrum with multiplicity >4 is in good agreement with the $87\pm5\%$ derived from the background-corrected spectrum in Fig. 4.

to the experimental spectrum shown in Fig. 6 confirmed that the resulting ratio was stable. It was found that 81.5% of the observed events were due to captures on ^{181}Ta and 18.5% to captures on $^{180}Ta^{m}$. In Fig. 7 this $^{180}Ta^{m}$ component is compared with the first analysis, where the ^{181}Ta component was directly subtracted (see Fig. 4). The good agreement of both methods confirms that systematic uncertainties are well controlled.

2. Multiplicity distribution

The second important question concerns the fraction of capture events $^{180}Ta^{m}$ contained in the evaluated spectrum with $m \geqslant 5$. This fraction was determined by a detailed computer simulation of the entire experiment using the codes CASINO and GEANT [16]. These codes were used to simulate the sum-energy spectra of different instrumental multiplicities for neutron capture in both Ta isotopes as well as for the auxiliary calibrating reaction of neutron capture in Au.

The most important result of these simulations was that the amazing difference in multiplicity measured for $^{180}Ta^{m}$ and ^{181}Ta could be reproduced in the CASINO/GEANT simulations. While the average multiplicity of ^{181}Ta events of $m=4.4$ corresponds to the expected average for heavy nuclei, the result for $^{180}Ta^{m}$ of $m=6.2$ is the highest multiplicity ever measured with the Karlsruhe 4π BaF_2 detector.

It needs to be stressed that for both Ta isotopes the same $E1$ and $M1$ photon strength functions were postulated and that the same parameter adjustment had been used. The only different input information for the CASINO/GEANT simulations consisted in the choice of two parameters for the level-density formula according to the constant-temperature approach [17]. In view of the negligible difference in mass number, the CASINO/GEANT predictions of the sum-energy spectra for $^{180}Ta^{m}$ are, therefore, considered to be equally successful than those obtained for ^{181}Ta.

The simulated spectra are illustrated in Figs. 8 and 9 for both isotopes where the calculated spectra are combined in the same way as the experimental results in Fig. 4. Note that the simulated multiplicity distribution of ^{181}Ta and the measured values given in Fig. 4 agree almost perfectly. The direct comparison of simulated and measured data in Fig. 8 shows that even the spectrum shapes for different multiplicites are in excellent agreement. In this comparison, the calculated spectra are normalized to the experimental data only by a single number, namely by the integral number of events in the total sum-energy spectrum. Note that the integral spectrum (instrumental multiplicities 1–15) plotted in upper left panel of Fig. 9 exhibits significant broadening of the sum-energy peak due to electron converted transitions in about 40% of the cascades. This effect is reproduced by the CASINO/GEANT simulations.

The remarkable success of the simulation confirms that capture events on $^{180}Ta^{m}$ with multiplicity $m \geqslant 5$ are, indeed, detected with 83% efficiency, consistent with the $87\pm5\%$ derived directly from the measured spectra (see Fig. 4).

D. Cross section ratios

The cross section ratio of isotope X relative to the gold standard is given by

$$\frac{\sigma_i(X)}{\sigma_i(\mathrm{Au})} = \frac{Z_i(X)}{Z_i(\mathrm{Au})}\frac{\Sigma Z(\mathrm{Au})}{\Sigma Z(X)}\frac{\Sigma E(X)}{\Sigma E(\mathrm{Au})}\frac{N(\mathrm{Au})}{N(X)}\mathcal{F}_1\mathcal{F}_2. \qquad (1)$$

In this expression, Z_i is the count rate of channel i in the TOF spectrum, ΣZ is the TOF rate integrated over the interval

TABLE II. Fraction f of undetected capture events (in %) and the related correction factors F_1. [Derived from capture cascades calculated with the code CASINO [10]].

	Threshold in sum energy (MeV)		
	1.5	1.7	2.0
f(Au)	4.36	5.12	6.27
$f(^{180}\mathrm{Ta}^m)$	0.35	0.55	0.85
$f(^{181}\mathrm{Ta})$	1.76	2.29	3.11
$F_1(^{180}\mathrm{Ta}^m/\mathrm{Au})$	0.960	0.954	0.945
$F_1(^{181}\mathrm{Ta}/\mathrm{Au})$	0.974	0.971	0.967

used for normalization (indicated by the vertical lines in Figs. 2 and 3), ΣE is the total count rate in the sum-energy spectra for all multiplicities in this TOF interval. The respective sum-energy spectra are shown in Fig. 4. In case of ^{197}Au and ^{181}Ta these spectra were integrated for all multiplicities from the threshold at 1.7 MeV up to and slightly beyond the respective binding energy, and the corresponding sum ΣE was used in Eq. (1) (for a detailed discussion see Ref. [13]). For $^{180}\mathrm{Ta}^m$, only the spectrum with multiplicity $m \geqslant 5$ could be analyzed as mentioned above, and ΣE was obtained by adopting the result of the CASINO/GEANT simulation according to which this spectrum represents 83% of the total events (see Fig. 9).

The other quantities in Eq. (1) are the sample thickness N in atoms/barn, the correction $F_1=[(100-f(\mathrm{Au}))/(100-f(X)]$, which accounts for the undetected fraction of capture events f below the experimental threshold in sum energy, and F_2, the ratio of the multiple scattering and self-shielding corrections. Index X refers to the respective tantalum sample. The fraction of unobserved capture events f and the correction factor F_1 were calculated as described in Ref. [7]. The input for this calculation are the detector efficiency for monoenergetic γ rays in the energy range up to 10 MeV and the capture γ ray cascades as used in the CASINO/GEANT simulations. In case of gold the capture cascades were calculated with various sets of input parameters. The main difference in these calculations was that for describing the decay of the compound nucleus in some cases a pygmy resonance was considered in addition to the electric giant dipole resonance. Since the experimentally determined capture cascades were better reproduced, the data sets based on the pygmy resonance were adopted in the final analysis. On average the absolute f values for the gold sample agree within 0.3% with results based on calculated cascades of Reffo and Uhl that had been used in Ref. [18].

The correction factors F_1 listed in Table II were found to agree within 1.6% with the F_1 values calculated for the previous tantalum measurement with the Karlsruhe 4π BaF_2 detector [7]. Meanwhile, the solid angle of the detector array was improved from 94% to 96%, and the calculated efficiency for monoenergetic γ rays was replaced by measured data. Note that the f values for $^{180}\mathrm{Ta}^m$ are fairly small: the detection efficiency for this isotope is nearly 100% due to the large cascade multiplicity.

The corrections for neutron multiple scattering and self-shielding, F_2, could be neglected since the sample masses were $\approx$8 times smaller than in the previous measurement on natural tantalum [7], where this correction was $\approx$1% in the neutron energy range considered here.

IV. NEUTRON CAPTURE CROSS SECTIONS

The measured neutron capture cross section ratios of $^{180}\mathrm{Ta}^m$, ^{181}Ta, and of ^{197}Au are free of systematic differences with respect to different runs or evaluations [2]. This represents a successful test for the consistent treatment of the respective data sets, which were obtained under different experimental conditions, e.g., with respect to neutron spectra and signal-to-background ratios.

As in previous measurements with the 4π BaF_2 detector [4,5,19] the final cross section ratios were adopted from evaluation 2. The averaged results of runs I and II are compiled in Table III together with statistical, systematic, and total uncertainties. The energy bins are sufficiently fine to avoid systematic uncertainties in the calculation of the Maxwellian averaged cross sections (Sec. VI). In the energy

TABLE III. Final neutron capture cross section ratios of $^{180}\mathrm{Ta}^m$ and ^{181}Ta relative to ^{197}Au.

Energy Bin[a] (keV)	$\sigma(^{180}\mathrm{Ta}^m)/\sigma(^{197}\mathrm{Au})$	Uncertainty (%)			$\sigma(^{181}\mathrm{Ta})/\sigma(^{197}\mathrm{Au})$	Uncertainty (%)		
		Statistical	Systematic	Total		Statistical	Systematic	Total
10–12.5	3.54	39	5.1	39	1.32	6.2	0.5	6.2
12.5–15	1.55	67	5.1	67	1.43	5.7	0.5	5.7
15–20	3.70	19	5.1	20	1.39	3.4	0.5	3.4
20–25	3.39	17	5.1	18	1.44	2.9	0.5	2.9
25–30	2.51	15	5.1	16	1.37	2.4	0.5	2.5
30–40	2.87	9.1	5.1	10	1.33	1.7	0.5	1.8
40–50	2.38	9.1	5.1	10	1.30	1.6	0.5	1.7
50–60	2.76	7.6	5.1	9.2	1.26	1.6	0.5	1.7
60–80	2.51	6.4	5.1	8.2	1.25	1.4	0.5	1.5
80–100	2.73	8.1	5.1	9.6	1.25	2.4	0.5	2.5

[a]Energy bins as used for calculating the Maxwellian averaged cross section.

TABLE IV. Neutron capture cross sections of $^{180}Ta^m$ and ^{181}Ta (in mb).

Energy Bin[a] (keV)	$\sigma(^{97}Au)$[b]	$\sigma(^{180}Ta^m)$	$\sigma(^{181}Ta)$
10–12.5	1067±16	3772±1470	1408±90
12.5–15	878±13	1360±911	1255±74
15–20	739±11	2736±547	1027±38
20–25	600±9	2036±366	864±28
25–30	571±9	1431±229	780±23
30–40	500±8	1435±143	664±16
40–50	433±7	1032±103	562±13
50–60	390±6	1076±99	493±11
60–80	349±5	877±72	436±9
80–100	298±5	813±78	374±11

[a]As used for calculating the Maxwellian averaged cross sections.
[b]Based on the ^{97}Au data from literature [20,21].

range from 30 keV to 100 keV the uncertainties of the cross section ratios are ≈10% for $^{180}Ta^m$ and ≈2% for ^{181}Ta, but increase significantly at lower energies.

The experimental ratios were converted into absolute cross sections using the gold data of Macklin [20] after normalization by a factor of 0.989 to the absolute value of Ratynski and Käppeler [21] (Table IV). The total uncertainties of the resulting values have been obtained by adding the 1.5% uncertainty of the reference cross section of gold to the uncertainties of the respective cross section ratios.

The present results are compared with previous data in Figs. 10 and 11. Since there are no other experimental data for $^{180}Ta^m$, this comparison is restricted to the available calculated data sets. It is important to note that all previous calculations overestimate the measured $^{180}Ta^m$ cross section

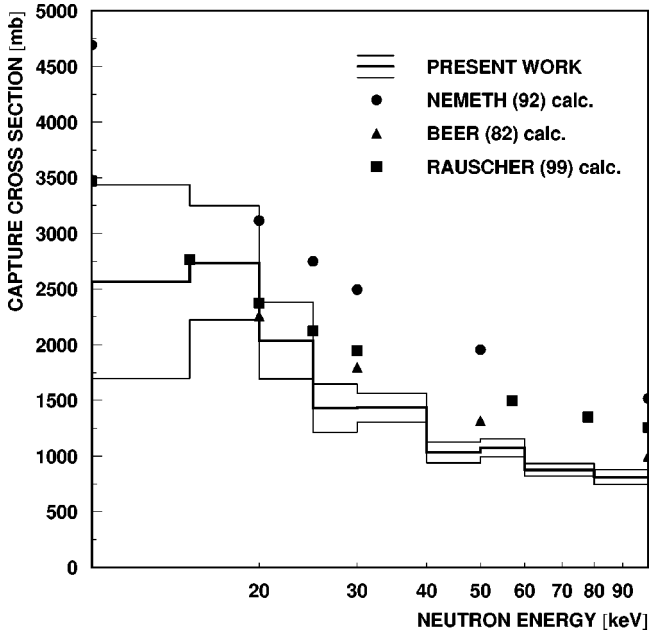

FIG. 10. The neutron capture cross section of $^{180}Ta^m$ compared to previous calculations [22–24].

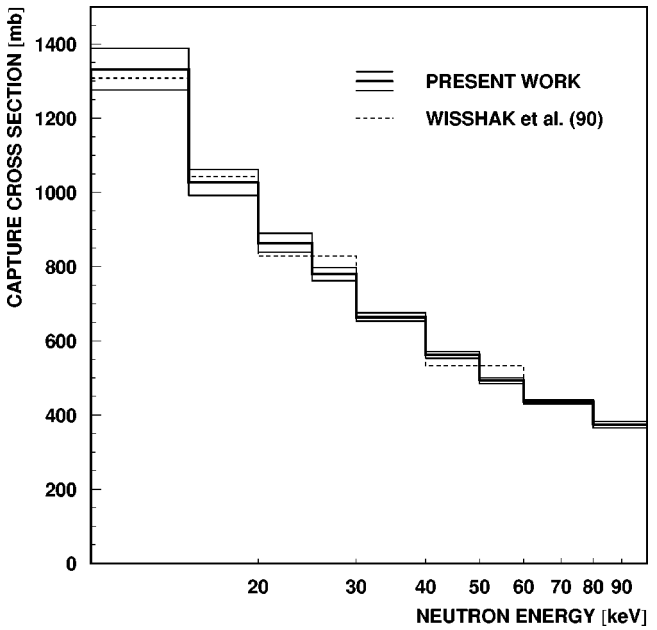

FIG. 11. The neutron capture cross section of ^{181}Ta compared to the previous measurement with the Karlsruhe 4π BaF_2 detector [7].

significantly. Obviously, statistical model calculations can be rather uncertain even for nuclei with high level densities. The calculations by Németh *et al.* [22] and Rauscher and Thielemann [23], which are based on local and global parameter systematics, respectively, yield nearly a factor of two larger cross sections than the experiment. In the calculation of Beer and Macklin [24] average radiation widths and level spacings deduced from data at thermal neutron energies were included [25,26], leading to a smaller discrepancy of about 20%.

The results for ^{181}Ta are in very good agreement with the cross sections obtained in the first experiment with the Karlsruhe 4π BaF_2 detector [7]. Since the previous measurement was performed with an eight times larger metallic sample without any additional container, the agreement with the present results confirms that the significant background due to scattered neutrons from the sample container was properly corrected.

V. DISCUSSION OF UNCERTAINTIES

The determination of statistical and systematic uncertainties in measurements with the 4π BaF_2 detector has been described in Refs. [4,5,7]. The following discussion emphasizes the particular aspects of the present experiment.

The binding energy for both investigated Ta isotopes and Au is sufficiently low for normalizing the scattering background in the sum-energy region around 9 MeV. This is crucial for the present experiment since this background is unusually large due to the graphite sample container. In this respect, it is important that the TOF dependence of this correction could be considered explicitly.

The absence of systematic differences in the data obtained in individual runs suggests that systematic uncertainties were well under control, similar to previous measurements

TABLE V. Systematic uncertainties (%).

Source of uncertainty	$\sigma(^{180}\mathrm{Ta}^m)/\sigma(^{197}\mathrm{Au})$	$\sigma(^{181}\mathrm{Ta})/\sigma(^{197}\mathrm{Au})$
Flight path	0.1	0.1
Neutron flux normalization	0.2	0.2
Sample mass:		
Elemental impurities	0.5	0.1
Isotopic composition	0.1	
Isotopic correction	0.2	
Multiple scattering and self-shielding: F_2	0.2	0.2
Undetected events: F_1	0.6	0.4
Number of events with multiplicity $\geqslant 5$	3.0	
Percentage of events with multiplicity $\geqslant 5$	4.0	
Total systematic uncertainties	5.1	0.5

[4,18,27]. This is confirmed by the agreement with the ^{181}Ta cross section of the first experiment [7], especially at low energies, where the signal-to-background ratio is crucial. The small systematic uncertainties related to the flight path and the neutron flux normalization have been discussed previously [5].

In the chemical analysis of the $^{180}\mathrm{Ta}^m$ sample, measurable impurities were only found for Na and Si at a level of 0.01%. For all other elements upper limits in the range from 0.02% to 0.05%were obtained. Since the most critical europium impurity was even below 0.005%, a systematic uncertainty of 0.5% was sufficient for neglecting the corrections for chemical impurities. In case of the natural tantalum oxide this uncertainty was only 0.1% The isotopic composition of the $^{180}\mathrm{Ta}^m$ sample (Table I) was specified with an absolute uncertainty of $<0.05\%$. In order to account for possible minor uncertainties in the determination of sample weight and stoichiometry, a total uncertainty of 0.1% was assumed for the sample mass.

The evaluation of the uncertainty related to the isotopic correction followed the procedure described for the gadolinium and dysprosium isotopes [18,27], yielding a total uncertainty of 0.2% for the present case.

The correction for multiple scattering and self-shielding was negligible due to the low sample mass. A corresponding uncertainty of 0.2% was adopted under the assumption that the graphite container affected the count rates of the tantalum and gold samples in the same way.

The systematic uncertainties due to undetected events were discussed in detail for the gadolinium experiment [18], where uncertainties of 0.3% for the even and 0.8% for the odd isotopes were estimated for the correction factor F_1. This

TABLE VI. Maxwellian averaged neutron capture cross section of $^{180}\mathrm{Ta}^m$.

ΔE	0–20 keV	20–100 keV	100–700 keV	Thermal spectrum			
kT (keV)	I_1, see text (mb)	I_2, see text (mb)	I_3, see text (mb)	$\langle\sigma v\rangle/vT$ (mb)			
					Statistical	Systematic[a]	Total
8	2550±178	509±50	0	3059	185	156	242
10	2009±140	686±61	0	2695	153	137	205
15	1211±84	926±70	6.0±0.3	2143	109	109	154
20	803±56	992±68	29±1.5	1824	88	93	128
25	569±40	974±63	70±3.5	1613	75	82	111
30	424±30	920±58	121±6.1	1465	66	75	100
40	261±18	781±47	227±11	1269	52	65	83
50	176±12	650±38	319±16	1145	43	58	72
52	165±12	626±37	334±17	1125	42	57	71
60	127±8.9	541±32	390±20	1058	39	54	67
70	958±6.7	454±26	443±22	993	35	51	62
80	749±5.2	385±22	482±24	942	33	48	58
90	601±4.2	330±19	510±26	900	32	46	56
100	493±3.5	285±16	529±26	863	31	44	54

[a]The 1.5% uncertainty of the gold standard is not included here, since it cancels out in most applications of relevance for nuclear astrophysics.

TABLE VII. Maxwellian averaged cross section of $^{180}Ta^m$ (in mb) at $kT=30$ keV compared to previous calculations and evaluations.

This work	Previous calculations		Evaluations	
1465 ± 100[a]	2355	2000 [23]	1800 ± 200	1987 [28]
	2662 ± 530	1992 [22]	1640 ± 260	2000 [29]
	1800 ± 200	1982 [24]		

[a]The 1.5% uncertainty of the gold cross section is not included, since it cancels out in most applications of relevance for nuclear astrophysics.

estimate was based on two independent sets of calculated capture cascades, and was found to agree with the respective uncertainties quoted in previous measurements with the 4π BaF_2 detector [4,5,19]. It turned out that this uncertainty was mainly determined by the difference in binding energy between the investigated isotope and the gold standard, which is large for the odd, but small for the even gadolinium isotopes. The same effect was observed for ytterbium [15]. According to this discussion, uncertainties of 0.6% and 0.4% are obtained for $^{180}Ta^m$ and ^{181}Ta, respectively.

In the present case, the overall systematic uncertainty is dominated by two additional corrections, which had to be considered because the $^{180}Ta^m$ analysis was exclusively based on events with multiplicity $m\geqslant5$. As described in Sec. IV the number of detected neutron captures on $^{180}Ta^m$ with $m\geqslant5$ was determined in two ways. First, the ^{181}Ta and $^{180}Ta^m$ components in the spectrum were separated by a fitting procedure derived from the systematics of sum-energy spectra (Fig. 6). The results obtained by this procedure differed systematically by 5% from the straightforward alternative, where the ^{181}Ta impurity was subtracted and the residuals integrated between the vertical lines in Fig. 7. Therefore, a systematic uncertainty of 3% was assumed for the finally adopted average of the two results.

In addition, the relative probability for $m\geqslant5$ events had to be determined. The rather uncertain fraction of $87\pm5\%$ (Fig. 4) was replaced in the final analysis by the $83\pm5\%$ obtained in the CASINO/GEANT simulation (Fig. 9). Based on the perfect agreement between experiment and simulation found for ^{181}Ta, the related uncertainty for $^{180}Ta^m$ was estimated to be 4%.

The systematic uncertainties are summarized in Table V. In contrast to previous studies, counting statistics plays a dominant role because of the comparably small sample mass (Table III).

VI. MAXWELLIAN AVERAGED CROSS SECTIONS

Maxwellian averaged cross sections were calculated as described in Refs. [5,7]. The neutron energy range from thermal to 700 keV was divided into three intervals according to the origin of the adopted cross sections.

The interval I_2 from 20 keV to 100 keV, which corresponds to the energy range of this experiment (Table IV), contributes $\approx$60% to the Maxwellian averaged cross section at $kT=30$ keV. The contributions I_1 and I_3 listed in Table VI were determined from the mean of the calculated cross sections of Németh *et al.* [22], Beer and Macklin [24], and Rauscher and Thielemann [23]. These calculated data sets were normalized to the present results in the neutron energy range from 20 keV to 80 keV, and their relative differences were used to derive the corresponding uncertainties.

The overall systematic uncertainties of the Maxwellian averaged cross sections include the uncertainties of the cross section ratios (Table III) and of the extrapolated components, I_1 and I_3. The 1.5% uncertainty of the gold standard was not included since it cancels out in most applications of relevance for *s*-process studies.

Since other experimental data are not available, the present results for $kT=30$ keV thermal energy are eventually compared in Table VII with previous calculations and with the compilations of Bao and Käppeler [28] and of Bao *et al.* [29]. The discrepancies between the present result and the previous calculations, which were noted for the energy-dependent cross sections, are also reflected in the Maxwellian averages. The recommended value of the recent compilation by Bao *et al.* [29], which is in fair agreement with the experiment, is not based on calculations but rather on the systematics of measured cross sections in the mass region around $A=180$.

ACKNOWLEDGMENTS

We are indebted to G. Rupp for his indispensable help with the experimental setup as well as E.-P. Knaetsch, D. Roller, and W. Seith for maintaining excellent beam conditions throughout the entire experiment. This work was partly supported by the Grant Agency of the Czech Republic under Grant No. 202/03/P136.

[1] H. Palme and H. Beer, in *Astronomy and Astrophysics*, edited by O. Madelung, Landolt-Börnstein, New Series, Group VI, Vol. 6, Part 3a (Springer, Berlin, 1993), p. 196.
[2] K. Wisshak *et al.*, Forschungszentrum Karlsruhe, Technical Report No. FZKA-6362, 2000.
[3] K. Wisshak *et al.*, Phys. Rev. Lett. **87**, 251102(4) (2001).
[4] K. Wisshak *et al.*, Phys. Rev. C **48**, 1401 (1993).
[5] K. Wisshak, F. Voss, F. Käppeler, and G. Reffo, Phys. Rev. C **45**, 2470 (1992).
[6] K. Wisshak *et al.*, Nucl. Instrum. Methods Phys. Res. A **292**, 595 (1990).
[7] K. Wisshak, F. Voss, F. Käppeler, and G. Reffo, Phys. Rev. C **42**, 1731 (1990).
[8] D. Belic *et al.*, Phys. Rev. Lett. **83**, 5242 (1999).
[9] D. Belic *et al.*, Phys. Rev. C **65**, 035801 (2002).
[10] F. Bečvář, in *Gamma-Ray Spectroscopy and Related Topics*,

edited by S. Wender (American Institute of Physics, New York, 2000), p. 504.
[11] M. Heil *et al.*, Nucl. Instrum. Methods Phys. Res. A **459** , 229 (2001).
[12] F. Bečvář, Nucl. Instrum. Methods Phys. Res. A **417**, 434 (1998).
[13] K. Wisshak*et al.* Forschungszentrum Karlsruhe, Technical Report No. FZKA-5967, 1997.
[14] K. Wisshak, R. Reifarth, F. Voss, and F. Käppeler, Forschungszentrum Karlsruhe, Technical Report No. FZKA-6694, 2001.
[15] K. Wisshak *et al.*, Phys. Rev. C **61**, 065801 (2000).
[16] J. Apostolakis, GEANT library, CERN, Technical Report, 1993, see http://wwwinfo.cern.ch/asd/geant/
[17] T. von Egidy, T. H. Schmidt, and A. Behkami, Nucl. Phys. **A481**, 189 (1988).
[18] K. Wisshak *et al.*, Phys. Rev. C **52**, 2762 (1995).
[19] F. Voss *et al.*, Phys. Rev. C **50**, 2582 (1994).
[20] R. Macklin (private communication).
[21] W. Ratynski and F. Käppeler, Phys. Rev. C **37**, 595 (1988).
[22] Z. Németh, F. Käppeler, and G. Reffo, Astrophys. J. **392**, 277 (1992).
[23] T. Rauscher and F.-K. Thielemann, At. Data Nucl. Data Tables **75**, 1 (2000).
[24] H. Beer and R. Macklin, Phys. Rev. C **26**, 1404 (1982).
[25] J. Mughabghab, M. Divadeenam, and N. Holden, *Neutron Cross Sections, Part A* (Academic, New York, 1981), Vol. 1.
[26] J. Harvey, N. Hill, and E. Mapoles, Oak Ridge National Laboratory, Technical Report ORNL-5025, 1975.
[27] F. Voss *et al.*, Phys. Rev. C **59**, 1154 (1999).
[28] Z. Bao and F. Käppeler, At. Data Nucl. Data Tables **36**, 411 (1987).
[29] Z. Bao *et al.*, At. Data Nucl. Data Tables **76**, 70 (2000).